Controlled Synthesis of 2D Palladium Diselenide for Sensitive Photodetector Applications

Long-Hui Zeng, Di Wu, Sheng-Huang Lin, Chao Xie, Hui-Yu Yuan, Wei Lu, Shu Ping Lau, Yang Chai, Lin-Bao Luo,* Zhong-Jun Li,* and Yuen Hong Tsang*

Palladium diselenide ($PdSe_2$), a thus far scarcely studied group-10 transition metal dichalcogenide has exhibited promising potential in future optoelectronic and electronic devices due to unique structures and electrical properties. Here, the controllable synthesis of wafer-scale and homogeneous 2D $PdSe_2$ film is reported by a simple selenization approach. By choosing different thickness of precursor Pd layer, 2D $PdSe_2$ with thickness of 1.2–20 nm can be readily synthesized. Interestingly, with the increase in thickness, obvious redshift in wavenumber is revealed by Raman spectroscopy. Moreover, in accordance with density functional theory (DFT) calculation, optical absorption and ultraviolet photoemission spectroscopy (UPS) analyses confirm that the $PdSe_2$ exhibits an evolution from a semiconductor (monolayer) to semimetal (bulk). Further combination of the $PdSe_2$ layer with Si leads to a highly sensitive, fast, and broadband photodetector with a high responsivity (300.2 mA W^{-1}) and specific detectivity ($\approx 10^{13}$ Jones). By decorating the device with black phosphorus quantum dots, the device performance can be further optimized. These results suggest the as-selenized $PdSe_2$ is a promising material for optoelectronic application.

1. Introduction

The rising star of 2D layered materials (transition metal dichalcogenide, TMDs) with unique properties has intrigued tremendous research interests worldwide owning to promising applications in various electronics and optoelectronics devices.[1–4] Graphene, as the first discovered 2D material with ultrahigh mobility, has offered great hope for technological applications in many areas, but the absence of inherent bandgap limits its practical application in photo/optoelectronic.[5–8] The advent of layered semiconducting TMDs including MoS_2, WS_2, $MoSe_2$, and WSe_2 with tunable bandgap ranging from 1 to 2 eV offers possible solution to issue.[9] However, it is relatively difficult to tailor bandgaps of these materials in a wide range, which constitutes a bottleneck for their device applications.[10,11] Black phosphorus, a recently extensively studied 2D layered material, possesses high mobility and a widely tunable bandgap variation from 0.3 to 2 eV, but it is highly unstable in air.[12–14] Therefore, it is greatly important to develop new 2D layered materials to address the drawbacks mentioned above.

Palladium diselenide ($PdSe_2$), a newly discovered group-10 TMD with unique crystal structure has thus far been scarcely investigated.[15–17] Although previous studies have shown that monolayer or few-layer $PdSe_2$ flakes can be promising building components for assembling powerful electrical devices such as field effect transistor,[15,18] it is undeniable that the fabrication of $PdSe_2$ is yet highly challenging. To date, the synthetic methods to acquire 2D $PdSe_2$ layer are still limited to mechanically assisted exfoliation,[15,18] and molecular beam epitaxy growth.[17] Unfortunately, these methods are featured with either low reproducibility, or uncontrollablity, which are clearly not suitable for practical applications. Thereby, it is highly desirable to develop a facile and proper approach to produce a large-area $PdSe_2$ film with high quality for next-generation

L.-H. Zeng, Prof. Y. H. Tsang
The Hong Kong Polytechnic University Shenzhen Research Institute
Shenzhen, Guangdong, China
E-mail: Yuen.Tsang@polyu.edu.hk
L.-H. Zeng, Dr. S.-H. Lin, Prof. S. P. Lau, Prof. Y. Chai, Prof. Y. H. Tsang
Department of Applied Physics
The Hong Kong Polytechnic University
Hung Hom, Kowloon, Hong Kong, China
Dr. D. Wu
School of Physics and Engineering
and Key Laboratory of Material Physics of Ministry of Education
Zhengzhou University
Zhengzhou, Henan 450052, China

Dr. C. Xie, Prof. L.-B. Luo, Prof. Z.-J. Li
School of Electronic Science and Applied Physics
Hefei University of Technology
Hefei, Anhui 230009, China
E-mail: luolb@hfut.edu.cn; zjli@hfut.edu.cn
Dr. H.-Y. Yuan
School of Materials Science and Engineering
Zhengzhou University
Zhengzhou, Henan 450052, P. R. China
Dr. W. Lu
University Research Facility in Materials Characterization and Device Fabrication
The Hong Kong Polytechnic University
Hung Hom, Kowloon, Hong Kong, China

**ADVANCED
SCIENCE NEWS**
www.advancedsciencenews.com

**ADVANCED
FUNCTIONAL
MATERIALS**
www.afm-journal.de

device applications. Recently, a post-chalcogenation through selenization or sulfurization of the pre-deposited metal layer has been proven to be an ideal method for synthesizing Mo, W, and Pt-based TMDs. It does not only offer better control to film uniformity and thickness, but also afford a simple stage with controllable pattern process for directly preparing a large-area 2D layered film on various substrates.[19] Enlightened by these works, we here reported on the wafer-scale growth of high-quality $PdSe_2$ films with adjustable thickness ranging from 1.2 to 20 nm by a simple selenization of pre-depositing Pd layer. The 2D $PdSe_2$ layer exhibits an evolution from semiconductor (monolayer) to semimetal (50 layers), which is consistent with theoretical simulation based on density functional theory (DFT) calculation. By directly integrating a multilayered $PdSe_2$ film with n-type Si substrate, a high-performance heterojunction photodiode was fabricated. It is revealed that the as-assembled heterojunction is able to function as a self-driven and broadband photodetector, with a high on/off ratio ($\approx10^5$), responsivity of up to 300.2 mA W^{-1}, and specific detectivity ($\approx10^{13}$ Jones), which are comparable to, or even higher than other 2D TMDs-based devices. Furthermore, by decorating the $PdSe_2$/Si heterojunction with black phosphorus quantum dots (BPQDs), the performance of BPQDs@PdSe/Si device can be optimized. The generality of the above results verifies that the as-selenized $PdSe_2$ material may find potential application in next-generation optoelectronic devices and systems.

2. Results and Discussion

The 2D $PdSe_2$ layer was obtained by a simple selenization process. Since the thickness of $PdSe_2$ is determined by the Pd layer, we can readily tune the thickness layer of $PdSe_2$ by adjusting appropriate Pd. **Figure 1**a shows a number of $PdSe_2$ layers with thickness of 1.2, 2, 4, 8, 12, 16, and 20 nm, which were obtained by selenizing Pd layers with around 0.3, 0.5, 1, 2, 3, 4, and 5 nm thick, respectively. Obvious color evolution from light gray to ivory was observed, as the thickness of $PdSe_2$ films gradually increased from 1.2 to 20 nm (see the AFM image in the inset of Figure 1a). From the XRD pattern in Figure S1 in the Supporting Information, we know that the $PdSe_2$ has a pentagonal structure (JCPDF #11-0453) with $a = 5.75$, $b = 5.87$, and $c = 7.69$ Å.[20] Basically, the $PdSe_2$ crystallizes in an unique pentagonal manner, with waved Pd–Se layers which are held together by van der Waals (vdW) force in Figure 1b. Further Raman analysis in Figure 1c reveals four apparent peaks at ≈143, ≈205, ≈221, and ≈255 cm^{-1} due to A^1_g, A^2_g, B_{1g}, and A^3_g, respectively. The three peaks at low wavenumber correspond to the movement modes of Se atoms, while the strongest mode is related to the relative movement between Pd and Se atoms.[18] As previously observed in $PtSe_2$ and $PtTe_2$, all the four Raman peaks will redshift as the thickness increases from few-layer to multilayer.[21,22] Furthermore, due to the change in space group, two more peaks at 120.2 and 129.8 cm^{-1} will appear in the Raman spectra for 1.2 nm $PdSe_2$ (see Figure S2, Supporting Information).[15,18] In addition to the precise tuning of the thickness, another advantageous feature with this selenization method is scalable. Figure 1d compares the camera pictures of both 2-inch Si wafer and $PdSe_2$ layer on Si. From the Raman mapping

shown in Figure 1e, one can easily see that the Raman signal intensities at different points are close to each other, indicating the good uniformity of the as-synthesized $PdSe_2$ film. Additionally, the chemical composition of $PdSe_2$ was confirmed by the X-ray photoemission spectroscopy (XPS) shown in Figure S3 in the Supporting Information.

To reveal the thickness-dependent electrical property of as-grown $PdSe_2$ films, the optical absorption measurements were conducted. **Figure 2**a shows the extrapolation Tauc plots, from which one can easily find that with the increase in thickness, the optical band edge will shift to lower energy. Based on these results, the bandgap value as a function of different layer was calculated. As revealed in Figure 2b, the bandgap is 1.08 eV for the 1.2 nm. As the layer increases from 3 to 40 layers, the bandgap will gradually reduce to 0.29 eV. Specifically, when the layer number reaches 50 layers, the bandgap is close to 0, suggesting the evolution from semiconductor to semimetal. To further unveil the thickness-dependent energy band structure of the as-synthesized $PdSe_2$ film, ultraviolet photoemission spectroscopy (UPS) analysis was further performed. Figure 2c,d shows the UPS analysis of $PdSe_2$ layers with varied thickness, in which the work function (W_F) values are calculated to be 4.32, 4.45, 4.70, 4.83, 5.07, 5.16, and 5.27 eV for 1.2, 2, 4, 8, 12, 16, and 20 nm, respectively. What is more, the difference between the Fermi level (E_F) and valence band maximum (VBM) is estimated to be 0.50, 0.45, 0.35, 0.26, 0.10, 0.06, and 0.00 eV for 1.2, 2, 4, 8, 12, 16, and 20 nm, respectively. By adding VBM with bandgap, the conduction band minimum (CBM) of $PdSe_2$ can be obtained. Figure 2e summarizes the VBM, E_F, and CBM as a function of different thickness. Such a thickness-dependent electrical property suggests the easy tunability of $PdSe_2$ by synthetic approach, which is highly beneficial for developing various electrical and optoelectronic devices with different geometries.

In order to theoretically obtain electronic structures of $PdSe_2$ thin films, it is pivotal to study the vdW interaction between adjacent layers (**Figure 3**a,b). For bulk $PdSe_2$, by employing SCAN+rVV10 functional, the calculated lattice constants are $a = 5.73$, $b = 5.87$, and $c = 7.74$ Å, which agrees well with the experimental values mentioned above. During our simulation, we assembled several kinds of $PdSe_2$ with varied layer number (e.g., 5, 10, 20, 40, and bulk) in Figure 3c–g. Since the thickness of monolayer $PdSe_2$ is around 0.4 nm, the thickness of these multilayer $PdSe_2$ are 2, 4, 8, and 16 nm. It is obvious that all the $PdSe_2$ thin films possess indirect bandgap. Moreover, with the increase in thickness, the bandgap is observed to shrink gradually. Even though such an evolution of bandgap with the thickness is similar to what is observed by experimental results, it is undeniable that the simulated bandgap is relatively smaller than the experimental results (Figure 3h). Such a discrepancy in simulation and experiment is understandable considering the fact that precise descriptions of electronic structures of semiconductor materials often entails complicated theoretical methods, such as HSE06 and GW methods, which is helpful to fully consider many-body effects among electrons. As a matter of fact, the above large discrepancy will be substantially relieved when Heyd–Scuseria–Ernzerhof (HSE) hybrid functional was adopted (Figure S4, Supporting Information).
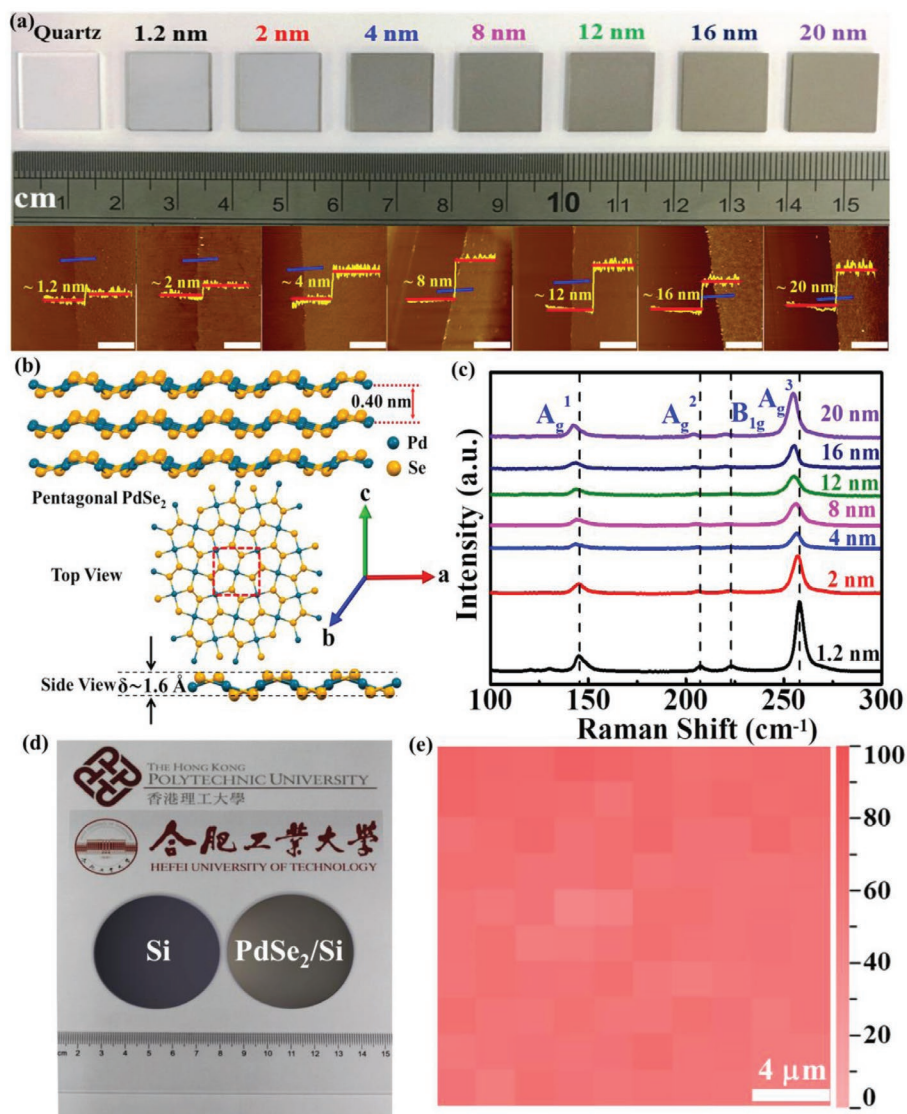
ADVANCED
SCIENCE NEWS
www.advancedsciencenews.com

ADVANCED
FUNCTIONAL
MATERIALS
www.afm-journal.de

Figure 1. a) Digital camera photo of PdSe$_2$ films with different thickness grown on the quartz, the bottom pictures show the corresponding AFM images, the all scale bars are 2 µm. b) Crystallographic structure of multi-layer and monolayer 2D PdSe$_2$. c) Raman spectra of PdSe$_2$ films with different thickness. d) Photographic image of Si wafer and PdSe$_2$ on Si wafer. e) Raman mapping image of PdSe$_2$ film obtained within an area of 20×20 µm^2, the intensity was normalized.

As mentioned above, the as-synthesized PdSe$_2$ film may display promising potential as building blocks for fabricating optoelectronic devices. To verify this assumption, we fabricated PdSe$_2$/n-Si heterojunction photodiodes by directly preparing a multilayered PdSe$_2$ film on silicon substrate. The inset of **Figure 4**a shows a typical photography of 4×4 heterojunction photodiodes (please refer to Experimental Section for more details about the device fabrication process). The cross-section high-resolution transmission electron microscopy (HRTEM) in Figure 4b exhibits the lattice-resolved image of the PdSe$_2$/Si interface, from which one can easily find that the multilay-ered structure has a thickness of around 20 nm. Since the layer distance is determined to be ≈0.40 nm according to the inset of Figure 4b, the layer number of PdSe$_2$ is around ≈50 layers with preferential orientation along [002] direction. Note that the PdSe$_2$ multilayer is not in intimate contact with the bottom

Si. Such a gap is probably formed during the sample prepara-tion process. In dark, the PdSe$_2$/Si heterojunction displays obvious rectifying effect with a high rectification ratio of ≈10^4 at ± 5 V. Considering the good Ohmic contact of Au/PdSe$_2$/Au and In-Ga/Si/In-Ga (Figure S5, Supporting Information), this rectifying behavior can be exclusively attributed to the PdSe$_2$/Si interface. Interestingly, once the heterojunction is shined by 780 nm light illumination, the current in the reverse bias will rise substantially (Figure 4c). This photosensitivity is reasonable that the built-in electric field (depletion region) in the PdSe$_2$/Si interface is able to separate the electron–hole pairs (Figure 4d).

Further optoelectronic characterization finds that with the increase in light intensity, the photocurrent of the PdSe$_2$/Si heterojunction will increase gradually (**Figure 5**a). Careful examination of the I–V curves under light illumination finds that the heterojunction actually demonstrates a weak
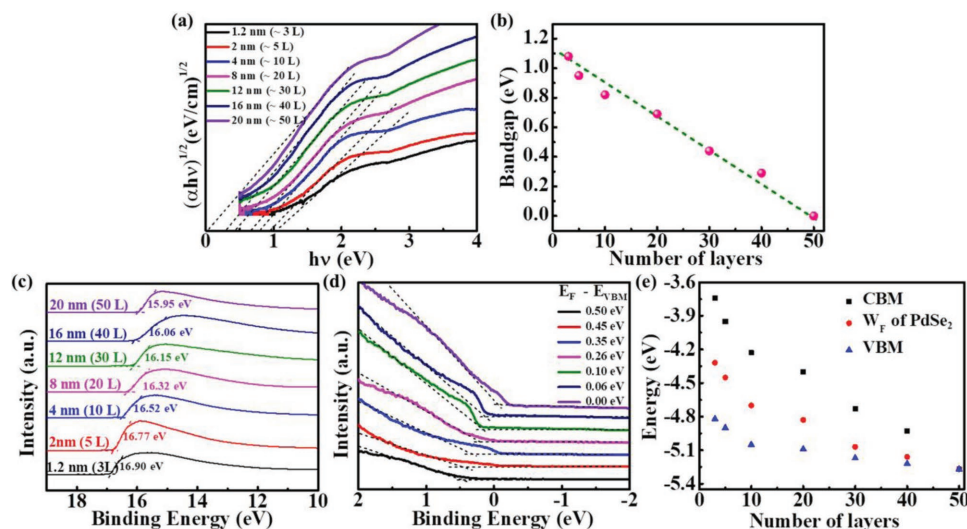
Figure 2. a) The Tauc plot of PdSe$_2$ with different thickness. b) The optical bandgaps extracted from Tauc plots for PdSe$_2$ with different layer numbers. c) Second electron cut-off regions. d) The energy difference between the Fermi level (E_F) and E_{VBM} extracted by UPS analysis. e) The CBM, E_F, and VBM as a function of different PdSe$_2$ layer number.

photovoltaic behavior: the photovoltage can increase from 52 to 350 mV when the incident light intensity increases from 0.9 µW cm^{-2} to 42.3 mW cm^{-2} in Figure 5b. The corresponding power conversion efficiency is relatively low, however, such a photovoltaic characteristic can facilitate the photodetection of light illumination under zero bias. Figure 5c displays the temporal photoresponse under alternative switching light with various light intensities at 0 V. Obviously, the PdSe$_2$-based device can be easily switched between on and off states, with a stable, repeatable, and high on/off ratio. Specifically, the on/off ratio of our device reached the maximum value of $\approx 1.08 \times 10^5$ under light intensity of 42.3 mW cm^{-2}. By fitting the relationship of light intensity and photocurrent with a power law of $I_{ph} \propto P^\theta$ (θ determines photocurrent response to the light intensity), a $\theta = 0.68$ was obtained (Figure 5d). The obtained value is smaller

than 1, signifying the presence of trap states in the device.[23] The responsivity (R) and specific detectivity (D^*) were calculated to quantitatively verify the performance of the present PdSe$_2$/Si photodetector, which are usually described by the following equations according to previous studies[24,25]

$$R(AW^{-1}) = \frac{I_p - I_d}{P_{opt}S} \tag{1}$$

$$D^* = A^{1/2}R/(2qI_d)^{1/2} \tag{2}$$

where I_p, I_d, P_{opt}, S, q, and A are the photocurrent, the dark current, the incident-light intensity, the effective illuminated area, the electronic charge, and the effective device area
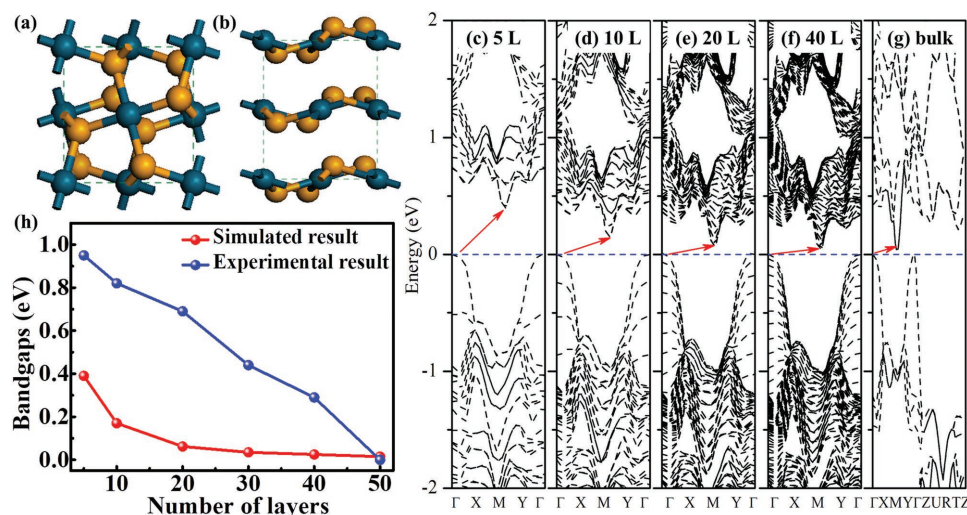

Figure 3. a,b) Top and side views of PdSe$_2$ film, the turquoise ball denotes the Pd atom, while the gold ball stands for Se atom. c–g) The simulated electronic band structure of PdSe$_2$ thin films with different thickness. h) The comparison of both experimental (blue) and theoretical (red) bandgap evolution of PdSe$_2$ with different thickness.
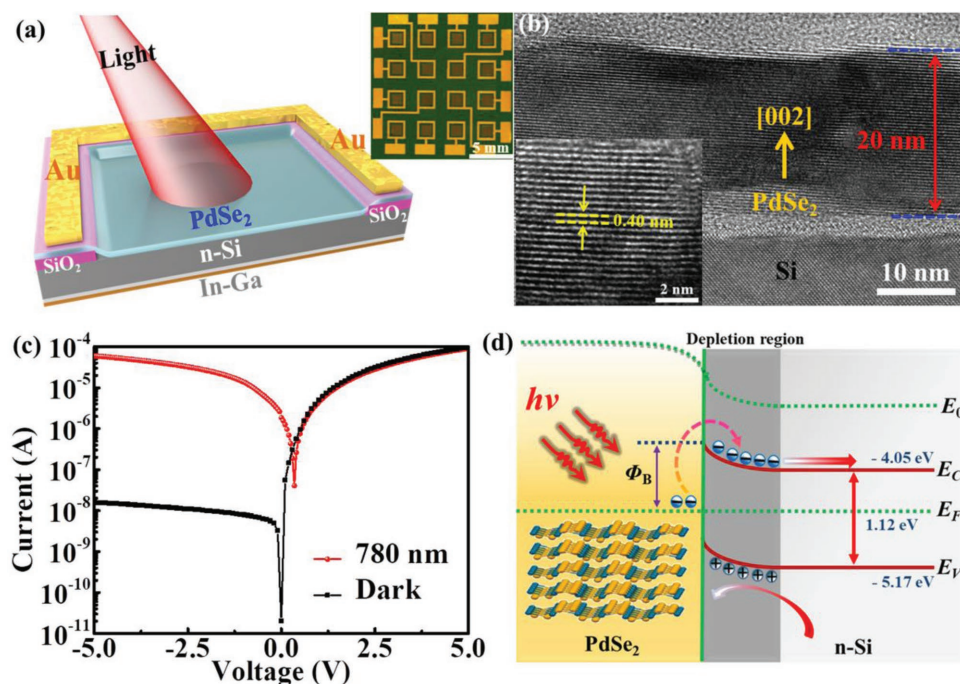
Figure 4. a) Schematic illustration (left) of PdSe$_2$/Si detector, and digital camera photography (right) of a device with 4 × 4 array devices. b) Cross-sectional TEM image of PdSe$_2$/Si structure and HRTEM image of the PdSe$_2$ layer (inset). c) The I–V curves of the PdSe$_2$/Si heterojunction device with and without 780 nm illumination, the light intensity is 42.3 mW cm^{-2}. d) Energy band diagrams of PdSe$_2$/Si heterojunction under light illumination at zero bias.

($A = S = 0.01$ cm^2), respectively. Therefore, R and D^* were calculated to be 300.2 mA W^{-1} and 1.18×10^{13} Jones, respectively, at low light intensity of 0.9 µW cm^{-2} at 0 V. The R value is comparable with the responsivity of graphene/Si Schottky junction photodetectors (270–730 mA W^{-1}) previously reported,[26–28] but it is better than that of PtSe$_2$ based photodetectors (10–262 mA W^{-1}).[29–31] Figure 5e shows the calculated R and D^* as a function of light intensity at zero bias. With the reduction of the incident light intensity, both values will increase. That is ascribed to increased carrier recombination activity under higher light intensity.[30] In this study, we totally fabricated 16 devices, all of which display relatively small fluctuation in photocurrent under identical light illumination (Figure 5f). This homogeneous distribution, along with the wafer-scale synthesis suggests good potential of the present PdSe$_2$/Si device for the development of large-area integrated optoelectronic systems in the future.[32]

In order to further optimize the photoresponse performance, the PdSe$_2$/Si heterojunction photodiode was intentionally functionalized with BPQDs, which have demonstrated promising application in a number of optoelectronic devices, especially in photodetectors.[17,33,34] **Figure 6**a shows the schematic illustration of a single BPQDs@PdSe$_2$/Si heterojunction photodetector. From the transmission electron microscopy (TEM) of BPQDs, it is obvious that BPQDs are uniformly distributed with an average diameter of ≈3.5 ± 0.5 nm (inset of Figure 6b). From the photoluminescence (PL) spectrum in Figure S6 in the Supporting Information, one can easily conclude that the BPQDs with bandgap of around 2.0 eV have been successfully decorated onto the PdSe$_2$ film. Figure 6c compares the I–V plots

of PdSe$_2$/Si with and without BPQDs decoration upon 780 nm excitation. Obviously, after decoration, the photocurrent of BPQDs@PdSe$_2$/Si is increased, owning to the enhancement of optical absorption. Moreover, we also study spectral response of heterojunction devices at different wavelength. As depicted in Figure 6d, both devices exhibit nearly identical photoresponse with maximum photocurrent peak at ≈920 nm and obvious cut-off wavelength around 1100 nm, which is the fingerprint of response spectrum of bottom n-Si, as shown in Figure S7 in the Supporting Information.[35] It is worth noting that, besides enhancement in 780 nm, the photocurrent in deep ultraviolet (DUV), near-infrared light (NIR), and even mid-infrared light (MIR) region were enhanced as well. Figure 6e,f shows the representative time-dependent photosensitivity under DUV (200 nm), NIR (2200 nm), and MIR (3044 nm) light illumination, respectively. Obviously, the photocurrent of our heterojunction devices under DUV, NIR, and MIR light illuminations with pronounced response are all enhanced by 1–2-folds. The enhancement in MIR photoresponse is possibly due to the defects in the BPQDs that are capable of absorbing IR light and forming photocurrent under IR illumination.[14,36,37] Another contributory factor is related to transition of electron from the valence band of BPQDs to the Fermi level of PdSe$_2$, which has been observed in other vdW heterojunction photodetectors made of MoTe$_2$–MoS$_2$,[38] WSe$_2$–MoS$_2$,[39] and so on. It should be pointed out that the BPQDs are not stable owing to their vulnerability of getting oxidized in ambient conditions. By this token, the present BPQDs functionalized photodetector can only keep its photosensitivity for less than couples of hours. To address this issue, we functionalize the BPQDs using
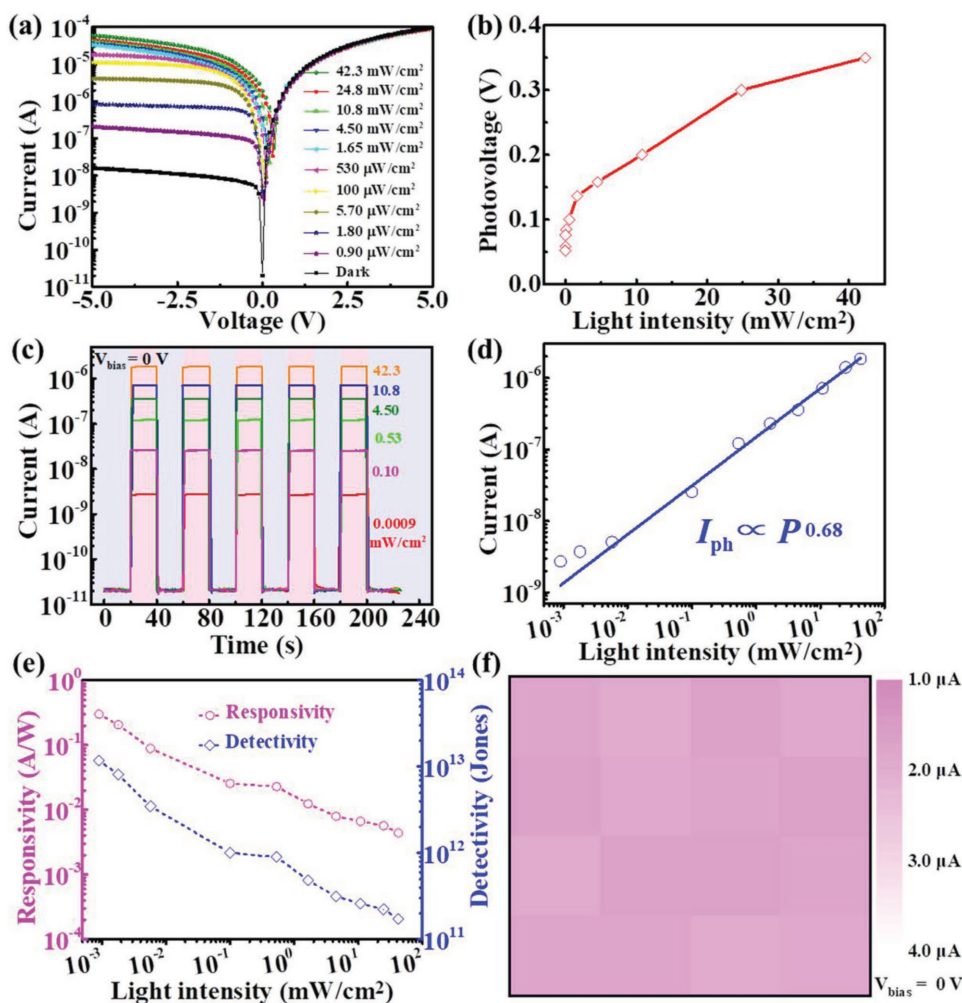
**ADVANCED
SCIENCE NEWS**
www.advancedsciencenews.com

**ADVANCED
FUNCTIONAL
MATERIALS**
www.afm-journal.de

Figure 5. a) I–V curves of the device at varied light intensities (780 nm). b) Photovoltage of the device as a function of power intensity. c) Photoresponse under various power intensities. d) The fitting of relationship between the photocurrent and power intensity at zero bias. e) R and D* as a function of light intensity. f) Photocurrent distribution of the 4 × 4 photodidoes.

simple titanium sulfonate ligand,[40] which are proved that can improve its ambient stability. According to our Raman spectrum in Figure S8 in the Supporting Information, the BPQDs after surface coordination display enhanced ambient stability (It will not get oxidized for 3 days). In addition, the as-coordinated BPQDs@PdSe$_2$/Si after exposure in air for 3 days shows only 10% decrease in photocurrent (Figure S9, Supporting Information), suggesting the relatively good air stability after surface coordination.

Apart from the high sensitivity to various wavelengths, the present BPQDs@PdSe$_2$/Si heterojunction photodiode exhibits a relatively fast response speed, which is comparable with that of other TMDs based detectors.[41–44] During the temporal response study, the pulsed optical signal was generated by 780 nm laser diode controlled by a function generator, and the transient photoresponse was recorded by an oscilloscope.[30,45] **Figure 7**a plots the photoresponse of the BPQDs@PdSe$_2$/Si hybrid heterojunction to pulsed light with different frequencies of 1, 5, and 10 kHz. Apparently, our photodetector exhibited fast switching response with good reproducibility for all measured frequencies.

However, at relatively high frequency (e.g., 5 and 10 kHz), the photoresponse experiences obvious degradation as a result of recombination due to trap densities in PdSe$_2$ thin film. The response speed of 38/44 μs (rise/fall time) for BPQDs@ PdSe$_2$/Si were determined from a single magnified photoresponse curve at frequency of 5 kHz, as shown in Figure 7b, according to the definition of response speed.[35,46] Such a response speed is comparable with that of WS$_2$/Si heterojunction (670/980 μs),[46] In$_2$Se$_3$/Si heterojunction (175/226 μs),[47] MoS$_2$/Si heterojunction (30.5/71.6 μs),[48] and graphene/Si Schottky junction (93/110 μs) in previous studies.[25] In addition, the relative balance $(V_{max} - V_{min})/V_{max}$ of the device verse different frequencies was shown in Figure 7c, indicative of a fast photoresponse with 3 dB bandwidth of ≈30 kHz. We believe this relatively quick speed is possibly related to special device geometry and built-in electric field, enhancing the fast separation and transport of photo-excited carriers.[49] As a matter of fact, we believe that this photoresponse speed could be further enhanced by reducing the photodiode capacitance or the thickness of plane Si substrate.[30,31]
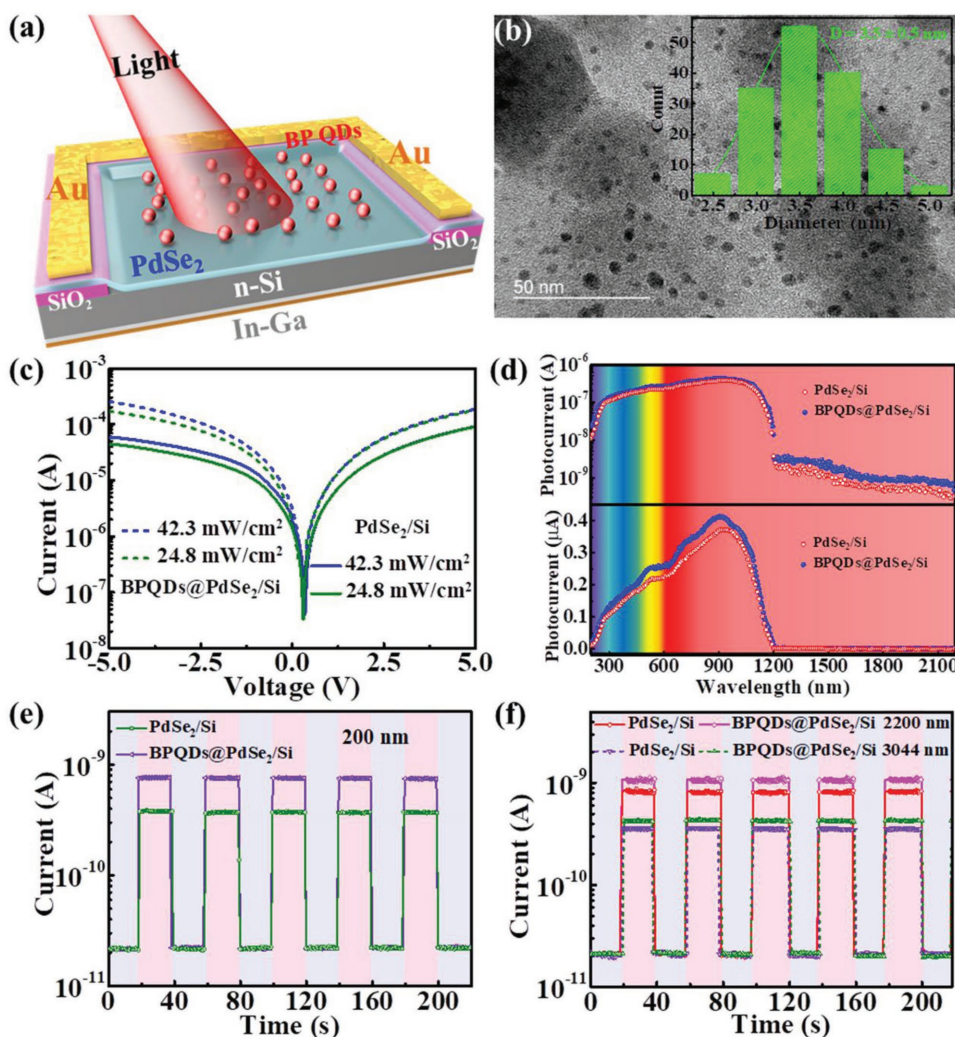
Figure 6. a) Schematic illustration of the BPQDs@PdSe$_2$/Si photodetector. b) TEM image of BPQDs with average diameter of 3.5 ± 0.5 nm. Statistical analysis of the lateral sizes of 160 BPQDs (inset). c) Associated current response for 780 nm light illumination. d) The spectral response of PdSe$_2$/Si with and without BPQDs decoration. Temporal photoresponse of PdSe$_2$/Si with and without BPQDs decoration under e) 200 nm (4.8 µW cm^{-2}), f) 2200 nm (150 mW cm^{-2}), and 3044 nm (100 mW cm^{-2}) light illumination at 0 V.

3. Conclusion

In summary, we have reported on the wafer-scale growth of 2D layered PdSe$_2$ with tunable thickness by simply selenizing pre-deposited Pd layer for the first time. The obtained PdSe$_2$ films are uniform and its thickness can be tailored from 1.2 to 20 nm by changing Pd metal layer. Optical absorption and UPS results confirm that PdSe$_2$ exhibits a gradual transition from a semiconductor (monolayer) to semimetal (bulk), which is consistent with theoretical simulation based on DFT. The as-grown PdSe$_2$ films could be a good candidate to form a fast and broadband heterojunction detector with Si, with a high responsivity (300.2 mA W^{-1}) and specific detectivity ($\approx 10^{13}$ Jones). Remarkably, the device performance can be further optimized through the decoration of BPQDs. These results suggest that the as-selenized PdSe$_2$ film as building blocks may find potential application in assembling next-generation optoelectronic systems in the future.

4. Experimental Section

Material Synthesis and Characterization: The PdSe$_2$ film was synthesized by a simple selenization. In brief, Pd metal layers were first deposited on SiO$_2$/Si (300 nm SiO$_2$ thickness) using magnetron sputtering system. The as-deposited Pd films were placed at the center zone of the growth furnace while selenium powder (99.99%) was at the upstream side. Selenium was evaporated at 220 °C in a 60 SCCM (standard cubic centimeter per minute) argon flow. The center of tube furnace was heated up to 480 °C and maintained for 90 min. The BPQDs in this study were prepared by an easy and widely used probe sonication with BP crystals in *N*-methyl-2-pyrrolidone and isopropyl alcohol solution.[50] The PL spectrum of BPQDs was measured by PL system equipped with a Xe Lamp (Edinburgh Photoluminescence). The absorption spectrum of PdSe$_2$ with different thickness on quartz glass was measured by a UV/VIS/NIR spectrometer. The Raman analysis was carried out on a Raman spectrometer, which uses 488 nm laser as excitation light. The XRD pattern was collected using a X-ray diffractometer. The XPS analysis was performed on a VG ESCALAB 220i-XL analysis system equipped with a monochromatic Al X-ray (1486.6 eV) source. The morphology, crystal structure of PdSe$_2$ and

ADVANCED
SCIENCE NEWS
www.advancedsciencenews.com

ADVANCED
FUNCTIONAL
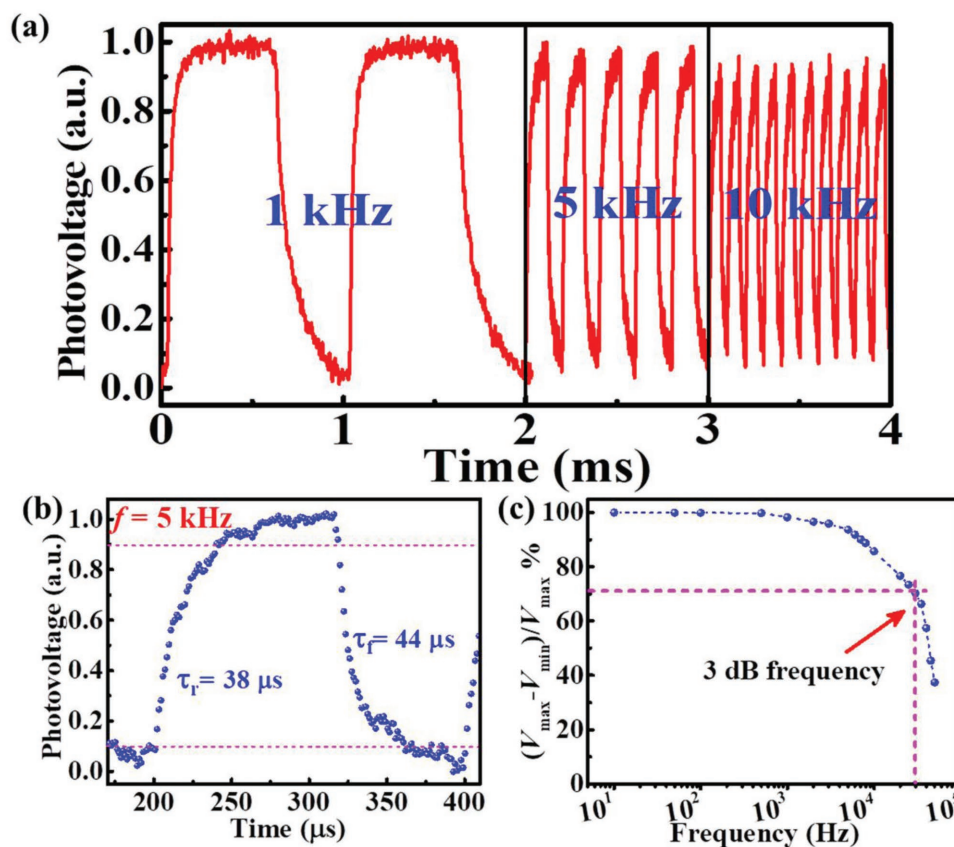MATERIALS
www.afm-journal.de

Figure 7. a) Photoresponse of the photovoltaic detector to pulsed light irradiation with a frequency of 1, 5, and 10 kHz. b) A single normalized cycle measured at 5 kHz to estimate response speed. c) Relative balance $(V_{max} - V_{min})/V_{max}$ versus input signal frequency, showing the 3 dB cut-off frequency of ≈30 kHz.

BPQDs were investigated using a field-emission transmission electron microscope (FETEM, JEOL Model JEM-2100F). The topography of PdSe$_2$ film was measured by AFM (VeecoNanoscope V).

Device Fabrication and Analysis: To fabricate the PdSe$_2$/Si photodetector, an exposed window (1 × 1 mm) was first defined on the SiO$_2$/n-Si (300 nm SiO$_2$, resistivity 1–10 Ωcm) wafer by photolithography, followed by etching in a buffered oxide etch solution for 5 min. After fabrication of 20 nm PdSe$_2$ film in the SiO$_2$/Si substrate with exposed area through the selenization method, 50 nm Au electrodes for PdSe$_2$ film and In-Ga alloy electrodes for Si substrate were prepared. To optimize the device performance of the PdSe$_2$/Si heterojunction detector, solution-processable BPQDs was decorated onto top surface of the PdSe$_2$ film by spin-coating method. The optoelectronic property was analyzed using a semiconductor I–V system (Keithley 4200-SCS) at room temperature, and a number of lasers with 780, 2200, and 3044 nm were employed as the irradiation source. To determine the time response of the heterojunction devices, the pulsed optical signal was generated by the 780 nm laser diodes equipped with a function generator (Tektronix, TDS2022B), and the photoresponse was examined via an oscilloscope (Tektronix, TDS2012B). During the spectral selectivity analysis, the monochromatic light was provided by a Xe lamp (CEL-HXF300) attached with a monochromator (Zolix Instruments, Omni-nx I).

Theoretical Method: The present first-principles calculations were carried out based on DFT using the Vienna ab initio simulation package. The generalized gradient approximation (GGA) in the Perdew–Burke–Ernzerhof (PBE) form was used for the exchange-correlation functional.[51] To evaluate the vdW interaction, the strongly constrained and appropriately normed (SCAN) meta-GGA functional was combined with the revised Vydrov–Van Voorhis long-range vdW correction functional (rVV10) in the course of simulation.[52–55] A kinetic-energy cut-off of 450 eV was chosen for the plane wave basis set to expand electronic wave functions. The PdSe$_2$ thin films can be cleaved from the (0001) surface of the bulk, and a vacuum region of 20 Å normal to the surface was added to remove the coupling between adjacent slabs. For the PdSe$_2$ thin films with the thickness of 5, 10, 20, 30, 40, and 50 layers (L), the 1 × 1 primitive cells were chosen, and the k-point samplings of 7 × 7 × 1 and 9 × 9 × 1 were used in geometrical optimization and electronic structure calculations, respectively. For bulk PdSe$_2$, a k-point sampling of 15 × 15 × 11 was employed in all calculations. Geometry structures were fully relaxed until the force on each atom was less than 0.01 eV Å^{-1}, and the convergence criteria was 10^{-5} eV for energy. Since the GGA-PBE method underestimates the bandgap of PdSe$_2$, the HSE06 functional was employed to calculate the bandgaps of PdSe$_2$ thin films.

Supporting Information

Supporting Information is available from the Wiley Online Library or from the author.

Acknowledgements

Conflict of Interest

The authors declare no conflict of interest.

Keywords

[1] C. Xie, C. Mak, X. Tao, F. Yan, *Adv. Funct. Mater.* **2017**, *27*, 1603886.

[2] M.-Y. Li, C.-H. Chen, Y. Shi, L.-J. Li, *Mater. Today* **2016**, *19*, 322.

[3] Y. Shi, H. Li, L. J. Li, *Chem. Soc. Rev.* **2015**, *44*, 2744.

[4] J. Wang, H. Fang, X. Wang, X. Chen, W. Lu, W. Hu, *Small* **2017**, *13*, 1700894.

[5] P. Avouris, C. Dimitrakopoulos, *Mater. Today* **2012**, *15*, 86.

[6] L. Zeng, L. Tao, C. Tang, B. Zhou, H. Long, Y. Chai, S. P. Lau, Y. H. Tsang, *Sci. Rep.* **2016**, *6*, 20343.

[7] O. Lopez-Sanchez, D. Lembke, M. Kayci, A. Radenovic, A. Kis, *Nat. Nanotechnol.* **2013**, *8*, 497.

[8] X. Yu, Y. Li, X. Hu, D. Zhang, Y. Tao, Z. Liu, Y. He, M. A. Haque, Z. Liu, T. Wu, Q. J. Wang, *Nat. Commun.* **2018**, *9*, 4299.

[9] F. H. Koppens, T. Mueller, P. Avouris, A. C. Ferrari, M. S. Vitiello, M. Polini, *Nat. Nanotechnol.* **2014**, *9*, 780.

[10] L. Ye, H. Li, Z. Chen, J. Xu, *ACS Photonics* **2016**, *3*, 692.

[11] J. Yin, Z. Tan, H. Hong, J. Wu, H. Yuan, Y. Liu, C. Chen, C. Tan, F. Yao, T. Li, Y. Chen, Z. Liu, K. Liu, H. Peng, *Nat. Commun.* **2018**, *9*, 3311.

[12] L. Li, W. Wang, Y. Chai, H. Li, M. Tian, T. Zhai, *Adv. Funct. Mater.* **2017**, *27*, 1701011.

[13] M. Buscema, D. J. Groenendijk, S. I. Blanter, G. A. Steele, H. S. van der Zant, A. Castellanos-Gomez, *Nano Lett.* **2014**, *14*, 3347.

[14] Q. Guo, A. Pospischil, M. Bhuiyan, H. Jiang, H. Tian, D. Farmer, B. Deng, C. Li, S. J. Han, H. Wang, Q. Xia, T. P. Ma, T. Mueller, F. Xia, *Nano Lett.* **2016**, *16*, 4648.

[15] A. D. Oyedele, S. Yang, L. Liang, A. A. Puretzky, K. Wang, J. Zhang, P. Yu, P. R. Pudasaini, A. W. Ghosh, Z. Liu, C. M. Rouleau, B. G. Sumpter, M. F. Chisholm, W. Zhou, P. D. Rack, D. B. Geohegan, K. Xiao, *J. Am. Chem. Soc.* **2017**, *139*, 14090.

[16] J. Sun, H. Shi, T. Siegrist, D. J. Singh, *Appl. Phys. Lett.* **2015**, *107*, 153902.

[17] E. Li, D. Wang, P. Fan, R. Zhang, Y.-Y. Zhang, G. Li, J. Mao, Y. Wang, X. Lin, S. Du, H.-J. Gao, *Nano Res.* **2018**, https://doi.org/10.1007/s12274-018-2090-0.

[18] W. L. Chow, P. Yu, F. Liu, J. Hong, X. Wang, Q. Zeng, C. H. Hsu, C. Zhu, J. Zhou, X. Wang, J. Xia, J. Yan, Y. Chen, D. Wu, T. Yu, Z. Shen, H. Lin, C. Jin, B. K. Tay, Z. Liu, *Adv. Mater.* **2017**, *29*, 1602969.

[19] Y. Jung, J. Shen, Y. Liu, J. M. Woods, Y. Sun, J. J. Cha, *Nano Lett.* **2014**, *14*, 6842.

[20] Y. Ma, L. Kou, X. Li, Y. Dai, T. Heine, *NPG Asia Mater.* **2016**, *8*, e264.

[21] M. Yan, E. Wang, X. Zhou, G. Zhang, H. Zhang, K. Zhang, W. Yao, N. Lu, S. Yang, S. Wu, T. Yoshikawa, K. Miyamoto, T. Okuda, Y. Wu, P. Yu, W. Duan, S. Zhou, *2D Mater.* **2017**, *4*, 045015.

[22] H. Ma, P. Chen, B. Li, J. Li, R. Ai, Z. Zhang, G. Sun, K. Yao, Z. Lin, B. Zhao, R. Wu, X. Tang, X. Duan, X. Duan, *Nano Lett.* **2018**, *18*, 3523.

[23] L. Wang, J. Jie, Z. Shao, Q. Zhang, X. Zhang, Y. Wang, Z. Sun, S.-T. Lee, *Adv. Funct. Mater.* **2015**, *25*, 2910.

[24] J. Mao, Y. Yu, L. Wang, X. Zhang, Y. Wang, Z. Shao, J. Jie, *Adv. Sci.* **2016**, *3*, 1600018.

[25] P. Lv, X. Zhang, X. Zhang, W. Deng, J. Jie, *IEEE Electron Device Lett.* **2013**, *34*, 1337.

[26] S. Riazimehr, A. Bablich, D. Schneider, S. Kataria, V. Passi, C. Yim, G. S. Duesberg, M. C. Lemme, *Solid-State Electron.* **2016**, *115*, 207.

[27] X. An, F. Liu, Y. J. Jung, S. Kar, *Nano Lett.* **2013**, *13*, 909.

[28] X. Li, M. Zhu, M. Du, Z. Lv, L. Zhang, Y. Li, Y. Yang, T. Yang, X. Li, K. Wang, H. Zhu, Y. Fang, *Small* **2016**, *12*, 595.

[29] Y. Zhao, J. Qiao, Z. Yu, P. Yu, K. Xu, S. P. Lau, W. Zhou, Z. Liu, X. Wang, W. Ji, Y. Chai, *Adv. Mater.* **2017**, *29*, 1604230.

[30] Z. X. Zhang, L. H. Zeng, X. W. Tong, Y. Gao, C. Xie, Y. H. Tsang, L. B. Luo, Y. C. Wu, *J. Phys. Chem. Lett.* **2018**, *9*, 1185.

[31] L.-H. Zeng, S.-H. Lin, Z.-J. Li, Z.-X. Zhang, T.-F. Zhang, C. Xie, C.-H. Mak, Y. Chai, S. P. Lau, L.-B. Luo, Y. H. Tsang, *Adv. Funct. Mater.* **2018**, *28*, 1705970.

[32] K. Kang, S. Xie, L. Huang, Y. Han, P. Y. Huang, K. F. Mak, C. J. Kim, D. Muller, J. Park, *Nature* **2015**, *520*, 656.

[33] G. Hu, T. Albrow-Owen, X. Jin, A. Ali, Y. Hu, R. C. T. Howe, K. Shehzad, Z. Yang, X. Zhu, R. I. Woodward, T. C. Wu, H. Jussila, J. B. Wu, P. Peng, P. H. Tan, Z. Sun, E. J. R. Kelleher, M. Zhang, Y. Xu, T. Hasan, *Nat. Commun.* **2017**, *8*, 278.

[34] C. Chen, N. Youngblood, R. Peng, D. Yoo, D. A. Mohr, T. W. Johnson, S. H. Oh, M. Li, *Nano Lett.* **2017**, *17*, 985.

[35] L. B. Luo, L. H. Zeng, C. Xie, Y. Q. Yu, F. X. Liang, C. Y. Wu, L. Wang, J. G. Hu, *Sci. Rep.* **2014**, *4*, 3914.

[36] X. F. Jiang, Z. Zeng, S. Li, Z. Guo, H. Zhang, F. Huang, Q. H. Xu, *Materials* **2017**, *10*, 210.

[37] T. Low, A. S. Rodin, A. Carvalho, Y. Jiang, H. Wang, F. Xia, A. H. Castro Neto, *Phys. Rev. B* **2014**, *90*, 075434

[38] K. Zhang, T. Zhang, G. Cheng, T. Li, S. Wang, W. Wei, X. Zhou, W. Yu, Y. Sun, P. Wang, D. Zhang, C. Zeng, X. Wang, W. Hu, H. J. Fan, G. Shen, X. Chen, X. Duan, K. Chang, N. Dai, *ACS Nano* **2016**, *10*, 3852.

[39] H. Fang, C. Battaglia, C. Carraro, S. Nemsak, B. Ozdol, J. S. Kang, H. A. Bechtel, S. B. Desai, F. Kronast, A. A. Unal, G. Conti, C. Conlon, G. K. Palsson, M. C. Martin, A. M. Minor, C. S. Fadley, E. Yablonovitch, R. Maboudian, A. Javey, *Proc. Natl. Acad. Sci. USA* **2014**, *111*, 6198.

[40] Y. Zhao, H. Wang, H. Huang, Q. Xiao, Y. Xu, Z. Guo, H. Xie, J. Shao, Z. Sun, W. Han, X. F. Yu, P. Li, P. K. Chu, *Angew. Chem., Int. Ed.* **2016**, *55*, 5003.

[41] D. Kufer, I. Nikitskiy, T. Lasanta, G. Navickaite, F. H. Koppens, G. Konstantatos, *Adv. Mater.* **2015**, *27*, 176.

[42] Z. Sun, H. Chang, *ACS Nano* **2014**, *8*, 4133.

[43] Q. Liu, B. Cook, M. Gong, Y. Gong, D. Ewing, M. Casper, A. Stramel, J. Wu, *ACS Appl. Mater. Interfaces* **2017**, *9*, 12728.

[44] X. Song, X. Liu, D. Yu, C. Huo, J. Ji, X. Li, S. Zhang, Y. Zou, G. Zhu, Y. Wang, M. Wu, A. Xie, H. Zeng, *ACS Appl. Mater. Interfaces* **2018**, *10*, 2801.

[45] L. H. Zeng, S. H. Lin, Z. Lou, H. Yuan, H. Long, Y. Li, W. Lu, S. P. Lau, D. Wu, Y. H. Tsang, *NPG Asia Mater.* **2018**, *10*, 352.

[46] C. Lan, C. Li, S. Wang, T. He, T. Jiao, D. Wei, W. Jing, L. Li, Y. Liu, *ACS Appl. Mater. Interfaces* **2016**, *8*, 18375.

[47] S. Chen, X. Liu, X. Qiao, X. Wan, K. Shehzad, X. Zhang, Y. Xu, X. Fan, *Small* **2017**, *13*, 1604033.

[48] Y. Zhang, Y. Yu, L. Mi, H. Wang, Z. Zhu, Q. Wu, Y. Zhang, Y. Jiang, *Small* **2016**, *12*, 1062.

[49] C. Xie, L. Zeng, Z. Zhang, Y. H. Tsang, L. Luo, J.-H. Lee, *Nanoscale* **2018**, *10*, 15285.

[50] S. Liu, S. Lin, P. You, C. Surya, S. P. Lau, F. Yan, *Angew. Chem., Int. Ed.* **2017**, *56*, 13717.

[51] J. P. Perdew, K. Burke, M. Ernzerhof, *Phys. Rev. Lett.* **1996**, *77*, 3865.

[52] J. Sun, A. Ruzsinszky, J. P. Perdew, *Phys. Rev. Lett.* **2015**, *115*, 036402.

[53] R. Sabatini, T. Gorni, S. de Gironcoli, *Phys. Rev. B* **2013**, *87*, 041108.

[54] O. A. Vydrov, T. Van Voorhis, *J. Chem. Phys.* **2010**, *133*, 244103.

[55] H. Peng, Z.-H. Yang, J. P. Perdew, J. Sun, *Phys. Rev. X* **2016**, *6*, 041005.